Title

Smartphone-interfaced lab-on-a-chip devices for field-deployable enzyme-linked immunosorbent assay

Journal

Biomicrofluidics, 8(6)

ISSN

1932-1058

Authors

Chen, Arnold

Wang, Royal

Bever, Candace RS

et al.

Publication Date

2014-11-01

DOI

10.1063/1.4901348

Peer reviewed

Smartphone-interfaced lab-on-a-chip devices for field-deployable enzyme-linked immunosorbent assay

Arnold Chen,[1] Royal Wang,[1] Candace R. S. Bever,[2] Siyuan Xing,[1] Bruce D. Hammock,[2,3] and Tingrui Pan[1,a)]
[1]*Department of Biomedical Engineering, University of California, Davis, California 95616, USA*
[2]*Department of Entomology and Nematology, University of California, Davis, California 95616, USA*
[3]*Comprehensive Cancer Center, University of California, Davis, California 95616, USA*

(Received 7 September 2014; accepted 30 October 2014; published online 5 November 2014)

The emerging technologies on mobile-based diagnosis and bioanalytical detection have enabled powerful laboratory assays such as enzyme-linked immunosorbent assay (ELISA) to be conducted in field-use lab-on-a-chip devices. In this paper, we present a low-cost universal serial bus (USB)-interfaced mobile platform to perform microfluidic ELISA operations in detecting the presence and concentrations of BDE-47 (2,2′,4,4′-tetrabromodiphenyl ether), an environmental contaminant found in our food supply with adverse health impact. Our point-of-care diagnostic device utilizes flexible interdigitated carbon black electrodes to convert electric current into a microfluidic pump via gas bubble expansion during electrolytic reaction. The micropump receives power from a mobile phone and transports BDE-47 analytes through the microfluidic device conducting competitive ELISA. Using variable domain of heavy chain antibodies (commonly referred to as single domain antibodies or Nanobodies), the proposed device is sensitive for a BDE-47 concentration range of 10^{-3}–10^{4} μg/l, with a comparable performance to that uses a standard competitive ELISA protocol. It is anticipated that the potential impact in mobile detection of health and environmental contaminants will prove beneficial to our community and low-resource environments. © *2014 AIP Publishing LLC*.
[http://dx.doi.org/10.1063/1.4901348]

I. INTRODUCTION

The rapid-growing usage of mobile technology in the world, both developing and developed countries, has greatly influenced the current development and future direction of healthcare diagnostic technologies.[1] With nearly 2.3×10^{9} mobile-broadband subscriptions in the world and 84 (per 100 inhabitants) in developed countries using smartphones,[2] an increasing amount of new healthcare devices (e.g., fitness, sleep, and vital sign monitoring) has been produced to work in complement with iPhones and/or Android phones.[3–5] Meanwhile, the revolution of miniature and portable chemical and biomolecular analytical systems has grown into what we know today as lab-on-a-chip (LOC) platforms capable of precise manipulation and rapid detection of a minute amount of analytes. Utilizing such microfluidic systems, conventional macroscale chemical and biological processes have been scaled down in terms of both sample size and device footprint. However, the majority of LOC devices is still restricted within a laboratory setting because of the bulky peripheral microcontrolling instruments and complicated detection schemes.

A truly portable, mobile, field deployable biochemical device has only recently been achieved through realization of high performing, hand-held microprocessors—Smartphones. Whitesides group first used a camera phone to take a picture of a colorimetric, paper-based glucose assay.[6] Soon after, detection of human IgG enhanced by visible gold nanoparticle silver staining in a

a)Author to whom correspondence should be addressed. Electronic mail: tingrui@ucdavis.edu

microfluidic immunoassay was also captured via a camera phone.[7] This initiated the concept of cellphone detection to which the Ozcan group greatly contributed by developing completely integrated bioanalytical systems with a phone camera.[8] Began with a phone microscope for imaging microparticles, blood cells, and parasites on glass slides,[9] the systems evolved to include fluorescence imaging and imaging processing apps.[10] Recently, a mobile phone system was reported to rapidly detect the presence of *Plasmodium falciparum*, an important biomarker for malaria, through electrochemical means.[11] Detection of environmental contaminants such as the level of mercury contents in water samples using a smartphone was also demonstrated.[12] The results were displayed on screen for immediate assessment proving its application as a mobile point-of-care (POC) diagnostic device that could be widely accessible in areas where the number of phone users continued to grow.

In terms of multistep biochemical assays, a portable detection setup of light-emitting diodes (LEDs), photodiodes, and LCD screen has developed to diagnose HIV and syphilis on a microfluidic device in a resource-limited environment.[13] The microfluidic chip was able to sample 1 μl of unprocessed whole blood and perform enzyme-linked immunosorbent assay (ELISA). Utilizing the bubble-based delivery mechanism, gas-segmented liquid reagent plugs in series replicated all conventional steps in a standard laboratory microplate protocol of ELISA. Implementing a chemical reduction process involving deposition of silver ions onto gold nanoparticles, assay results were visible to the eye and absorbance signals could be acquired.[13] Detection of bladder cancer biomarkers in urine has been demonstrated using a negative pressure driven microfluidic device for conducting bead-based ELISA.[14] In another effort, by miniaturizing standard 96 wells microplate system into a microfluidic configuration, an on-chip ELISA assay was improved in terms of sample and reagent conservation, reaction kinetics, and detection sensitivity.[15] However, the above mentioned microfluidic ELISA systems lacked portability and low cost for point-of-care applications in general, with the exception of Chin *et al.*, because the peripheral controlling/detection instruments of the microfluidic device were still expensive, bulky, and heavy. The microfluidic-microplate system typically required a plate reading/scanning machine.[15,16] In addition, a micro-ELISA for allergy diagnosis drew samples and reagents from a rotating tube stage with a syringe pump.[17] Microspot-based ELISA in microfluidics used a robotic spotter to add antibody solutions, a syringe pump to control flow in microfluidic channels, electronic systems for signal acquisition, and a computer for data processing.[18] Rapid, portable, bead-based microfluidic platform was shown to detect presence of *Carcinus maenas* (an environmentally damaging marine crab) by packing beads densely inside a small chamber to reduce diffusion rate[19] and diffraction-limited fluorescent could improve detection.[20] With progress in cellphone imaging and computing, a data readout mechanism could be implemented, however, the current pumping design needs to be replaced by a new integratable fluidic manipulation scheme to allow mobility.

Micropumps have been developed primarily for the purpose of providing transportation of micro/nanoscopic volume in enclosed microchannel networks; and it can be achieved through mechanical or non-mechanical principles.[21,22] Bubble gas generation is an electrochemical strategy for creating displacement through application of electrolysis, which is capable of producing large pressure with low energy consumption.[23–25] The design of electrodes has become interdigitated as the separation distance between anode and cathode electrodes is minimized to improve efficiency and reduce heat generation.[26–29] The material of the electrodes is often platinum and the electrolyte is commonly water as its molecules break down to oxygen and hydrogen gases.[28,30–33] The advantage of using water-based gas generating micropumps is biocompatibility, which allows its implementation in various biomedical applications including blood cell analysis,[29,34] glucose sensors,[35] and intraocular drug delivery.[36–38] Non-liquid phase bubble generation has been reported using manganese dioxide (MnO_2) powder to react with hydrogen peroxide[39–41] and sodium polyacrylate-based hydrogel containing 99 wt. % water that releases oxygen and hydrogen gases.[42]

In this paper, we present a low cost universal serial bus (USB)-interfaced mobile platform to control, execute, and read microfluidic-based immunoassays for healthcare-related applications. The completely portable system includes a smartphone for capturing real-time colorimetric images, which is then wirelessly transferred to a computing server for post image processing. The phone utilizes the USB interface to power an Arduino microcontroller that is uploaded with a script written to automatically supply voltage inputs serially to copper electrode pairs on

a printed circuit board (PCB) with a microfluidic chip insertion slot. Plug-and-play microfluidic chips have been fabricated to perform competitive ELISA operations in detecting the presence and concentrations of BDE-47 (2,2′,4,4′-tetrabromodiphenyl ether), the most prominently found species of the environmental contaminants polybrominated diphenyl ethers (PBDEs), using variable domain of heavy chain antibodies (VHH). Our point-of-care diagnostic configuration utilizes two sets of electrode pairs for interfacing electrical properties with biochemical behaviors: metal electrodes on the controlling module and carbon black composite material integrated on the microfluidic chip. Carbon black composite electrodes allow the microfluidic device to be low-cost, low-power, disposable, and less susceptible to electrochemical degradation than traditional metal electrodes.[43,44] On-chip interdigitated carbon electrodes act as micropumps by generating gas bubbles through electrolysis to produce volume expansion resulting in liquid displacement. Importantly, we have implemented the electrolytic control and pumping mechanisms to completely replicate an immunoassay (i.e., ELISA) procedure into a microscale, lab-on-a-chip format with comparable performance to the laboratory-based method.[45] In summary, our integrated mobile-interfaced POC system, as shown in Fig. 1, can be cost-effective, power-efficient, field-deployable, widely accessible, user-friendly, simple-to-use (plug-and-play), which could be offered as a generic biochemical detection platform in the future.

II. MATERIALS AND METHODS

A. Materials

The protein antigen used as the immobilized reagent on the sensor surface was a brominated diphenyl ether hapten conjugated to bovine serum albumin (BDE-C2-BSA) described previously.[46] The reagent used for detection was a VHH isolated from an alpaca, described here.[45,47] The VHH was directly labeled with horseradish peroxidase (HRP; EZ-Link Plus

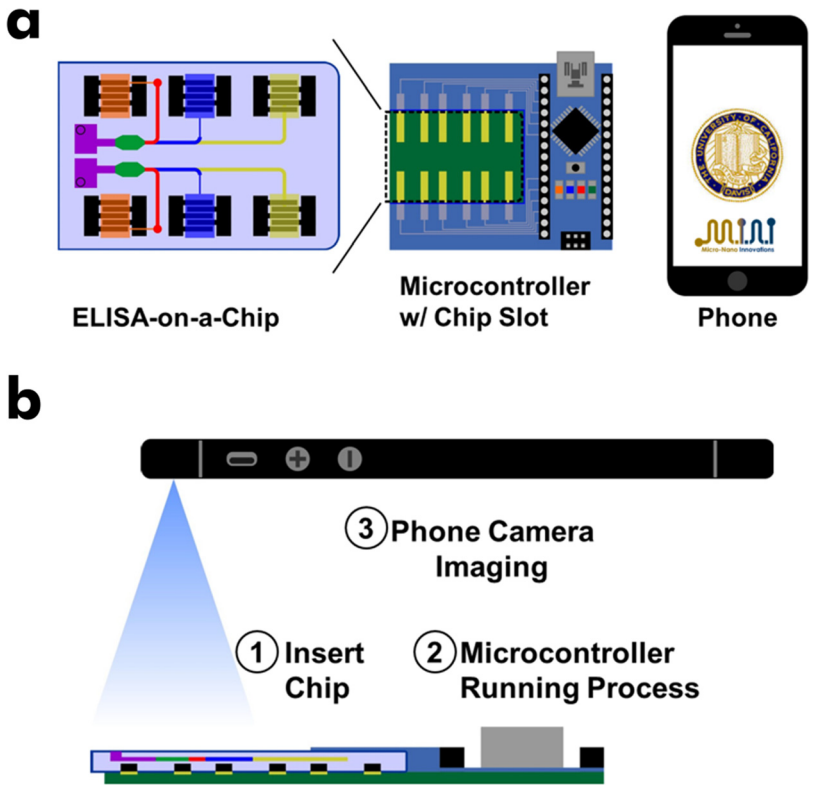

FIG. 1. (a) Integrated mobile-interfaced point-of-care system including a camera phone, an encased Arduino microcontroller on copper electrodes with a microfluidic chip slot, and a microfluidic ELISA-on-a-Chip. (b) Configuration with the microfluidic device inserted onto the copper electrodes and the phone camera imaging the ELISA reaction.

Activated Peroxidase, Pierce Biotechnology, Rockford, IL) in phosphate buffered saline (PBS) with slight modifications to the manufacturer's protocol. The VHH was mixed with activated HRP at a molar ratio of 4:1 due to the smaller size of the VHH protein.

B. Device fabrication

Microfluidic devices were microfabricated using polydimethylsiloxane (PDMS, Sylgard 184, Dow Corning) prepared at 10:1 curing agent to base polymer ratio. PDMS of 1.0 mm height were cured on 50 mm by 75 mm glass slides at 100 °C for 1 h. The PDMS device is 25.4×38 mm. Afterwards, channels, chambers, and through-holes were etched out of the PDMS material by a desktop CO_2 laser engraver (VersaLaser, Universal Laser Systems). Micropump chambers are $4.0 \times 5.0 \times 1.0$ mm and 7.5 mm apart, the detection chambers are $2.0 \times 4.0 \times 0.5$ mm with tapering, the waste chambers are $4.0 \times 4.0 \times 0.5$ mm, and the sample chamber has a 600 μm radius. The channels are all 200 μm deep with width of 250 or 500 μm. Long main channel is 19 mm, and branch channels to micropump chambers are 3.0 mm. All layers of the microfluidic device were fabricated through laser etching, i.e., top sample injection layer, middle microfluidic channel network layer, and bottom electrode layer. After laser etching, the electrode layer had an additional deposition step of carbon black composite material into designated $150\ \mu\text{m} \times 4.0$ mm interdigitated regions. Carbon electrodes were made by mixing carbon black (with an average diameter of 50 nm, Vulcan® XC72R, Cabot) with PDMS to generate C-PDMS with composition from 5% to 25% carbon by total weight. C-PDMS mixture was first loaded into the patterned electrode recesses, and successively, a plastic squeegee was used to remove excess C-PDMS residuals on the surface, followed by curing at 100 °C for 1 h. Once embedded with C-PDMS electrodes, the electrode layer was oxygen plasma-treated (30 W for 20 s) and bonded to the middle microfluidic layer with an alignment procedure under a microscope. The middle microfluidic network layer then had its chambers surface-modified with a protein antigen of BDE-C2-BSA. At the last step, the top PDMS layer was treated with PDMS cross-linking agent and put in contact with the already bonded middle-bottom layer assembly.[48,49]

C. Protein surface modification

The PDMS detection chambers were first treated with 10% 3-aminopropyl-triethoxysilane (APTES) in ethanol for 10 min and then baked on a 125 °C hotplate for 20 min. Afterwards, the PDMS layer was rinsed with ethanol and air dried prior to treatment with 1% glutaraldehyde in PBS for 1 h. The PDMS device was then rinsed with deionized (DI) water and dried. Antigen BDE-C2-BSA (10 μg/ml) was introduced to the treated detection chambers, was washed with PBS after 1 h, and finally air dried. Substituting the antigen, bovine serum albumin (BSA) of 10 μg/ml was coated in the adjacent detection chamber to serve as control.

D. Microfluidic competitive ELISA protocol

An electrolytic solution 0.5 M KNO_3 was loaded into each electrolyte chamber via needle injection. Sample analyte BDE-47 was premixed with VHH αBDE-47 (4 μg/l) to reach a concentration ranging from 10^{-3} to 10^4 μg/l and added to the sample chambers. VHH were directly labeled with HRP, eliminating the need of secondary antibodies for signal visualization. The last electrolyte chamber contained a mixture of enzymatic substrate (98% citrate, 1.6% 3,3′,5,5′-tetramethylbenzidine (TMB), 0.4% H_2O_2) with KNO_3 for colorimetric measurements. When 5 V was supplied, electrolytic reaction generated H_2 and O_2 gases to push sample analytes into the detection chamber. After a 10 min incubations, electrolytic pumping reaction from a second chamber washed unbound antibodies away for 2 min.[50] The final electrolysis micropump added an enzymatic substrate solution to the detection chamber for colorimetric analysis.

E. Data acquisition and imaging processing

Camera photographs of the ELISA colorimetric readings were taken in .jpeg format and wirelessly sent to a computer for data processing. ImageJ software was used to extract red,

green, and blue (RGB) values of the detection chambers ($2 \times 2\,mm^2$). Each sample value had BSA control value subtracted and then normalized. For both the conventional assay and the LOC device, a total of 8 different BDE-47 concentrations were measured. Each concentration point in the LOC curve had triplicate measurements.

III. RESULTS AND DISCUSSION

A. Conductivity of carbon-PDMS

C-PDMS electrodes have been fabricated at 5%–25% composition by adding carbon black to PDMS prior to the curing step. As the amount of carbon black increased, C-PDMS becomes more viscous until it behaves like a moldable solid. We stopped at 25% composition as the composite material reaches saturation and further addition of carbon black powders are not absorbed.[43] This is a physical limitation of combining carbon black powders with PDMS material. In addition, a higher power ratio of the C-PDMS makes the composite material more brittle mechanically.[51] The conductivities of C-PDMS with various weight ratios of carbon powders have been characterized and summarized in Fig. 2 where integrated electrode pairs of $1 \times 1 \times 2\,mm^3$ have been used. At a lower carbon content, the carbon particles embedded within the PDMS can be distributed farther from each other due to low packing density. Carbon particles not in direct vicinity of each other therefore cannot exchange electrons/charges to generate any current flow. As the content of carbon particles increases to a density where the particles are in physical contact, flow of electrons/charges from one end of the electrode to the other is observed, known as the percolation limit/threshold.[52] Further increase in particle density creates a network of flow path that readily conducts current.[53] As expected, a higher conductivity has been achieved at a higher carbon ratio of the C-PDMS composition with the highest value of 15 S/m at 25%. There are several advantages of using C-PDMS as electrodes as opposed to conventional metal electrodes (e.g., platinum, gold, chromium, and titanium). C-PDMS materials are an affordable alternative to the conventional metal electrodes as these inexpensive conductive polymers are capable of permitting the flow of current. Importantly, preparation of C-PDMS does not introduce additional complexity to the existing PDMS processing (e.g., electrode plating) while retaining its ability to bond and seal to glass substrates containing pressurized flows. According to our observations, as well as previous investigations, these electrodes are able to withstand a large range of electric field intensities (up to 37.5×10^4 V/m) and frequencies (up to 300 kHz) without degradation or release of any carbon particles.[43]

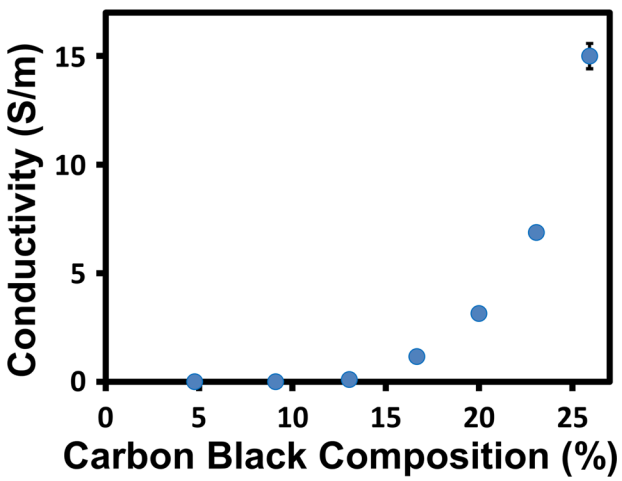

FIG. 2. Characterization of the carbon-PDMS electrodes. The conductivity of the carbon-PDMS composite material is measured with respect to the amount of carbon black material in the mixture.

B. USB—microfluidic chip interface

C-PDMS were in contact with copper electrodes on a PCB to allow flow of current for powering the electrolysis micropumps. Copper electrodes were connected to an Arduino controlling board for automatic operations of multiple electrolysis micropumps in sequential order. The Arduino Nano was powered through a microUSB cable from a mobile phone. A simple Arduino script was written to supply voltage (5 V) to 3 pins (i.e., 1, 2, and 3) independently and sequentially. When voltage is supplied to pin 1, current flows from the Arduino to the PCB electrodes and to the C-PDMS electrodes resulting in electrolytic chemical reaction. Voltage stays for the duration of fluidic pumping and then is cut off to stop pumping. Moving on, the next micropump receives voltage from pin 2 to pump fluid and is also cut off when finished. Finally, the last micropump receives a voltage supply to pump and complete the fluidic operations.

C. Characterization of electrolytic micropump

Carbon-PDMS electrodes have been incorporated to generate electrolytic reactions for microfluidic manipulations, that is, producing expanding H_2 and O_2 gaseous bubbles with volume displacement to drive liquid movement. We utilize two interdigitated C-PDMS electrodes with an electrolytic solution of 0.5 M KNO_3 to pump fluids down microfluidic channels. Similar to other pressure-driven pumps, the electrolytic pump utilizes pressure generated from bubble expansion to displace fluids whose flow rate is influenced by the resistance of the microfluidic channel and from the back pressure. Essentially, the effectiveness of the pump is primarily determined by its ability of stably creating pressurized bubbles by an electrolytic reaction. By utilizing the KNO_3 electrolytes, gaseous bubbles nucleate more readily as voltage requirement is reduced in salt solutions.[29,54] Current flow is the driving force behind the electrochemistry. As the applied electrolytic current increases from 0 to 4 mA, the corresponding flow rate follows the rising trend almost linearly, increasing from 0 to 27.5 μl/min as shown in Fig. 3(a). The limitation of electrolytic micropump is a careful balance between microfluidic channel resistance and back pressure with the achievable range of bubble pressure. Separately, the consistency of the C-PDMS electrolytic micropump is determined by measuring pumping volume over time. As shown in Fig. 3(b), an electrolytic current of 1 mA is initially applied to produce a stable pumping rate of 3.08 μl/min over a 10 min period (i.e., the pump "ON" period), from which a steady-state increase in gaseous volume has been produced and collected by the C-PDMS micropump. After the pumping phase, the electrolytic current is shut off, stopping the micropump, which leads to an apparent instant volume plateau with a slight decrease in volume ($<$0.5 μl) possibility due to evaporation into the gas phase. In comparison, a micropump driven simply by water electrolysis without any salt content is susceptible to significant backflow in the absence of current source as hydrogen and oxygen gases passively re-equilibrate to form liquid phase water in the reverse electrolytic reaction.[36,38]

Subsequently, we have investigated the pump efficiency (η) in a range of applied electric current. According to the electrochemical theory, the electrolytic efficiency of a reaction can be evaluated as[32,36]

$$\eta = \frac{V_{experimental}}{V_{theoretical}}, \tag{1}$$

where $V_{experimental}$ and $V_{theoretical}$ are the actual volume and theoretical volume of generated hydrogen and oxygen gases, respectively. Moreover, theoretical volume $V_{theoretical}$ can be calculated by the following equation:[36]

$$V_{theoretical} = \frac{3}{4}\frac{V_m}{F} i\, t, \tag{2}$$

where the molar gas volume (V_m) at 25 °C and atmospheric pressure is 24.7 $\times$ 10^{-3} m^3/mol, the Faraday's constant (F) is 96,485 A s/mol, applied current (i) in ampere, and time duration

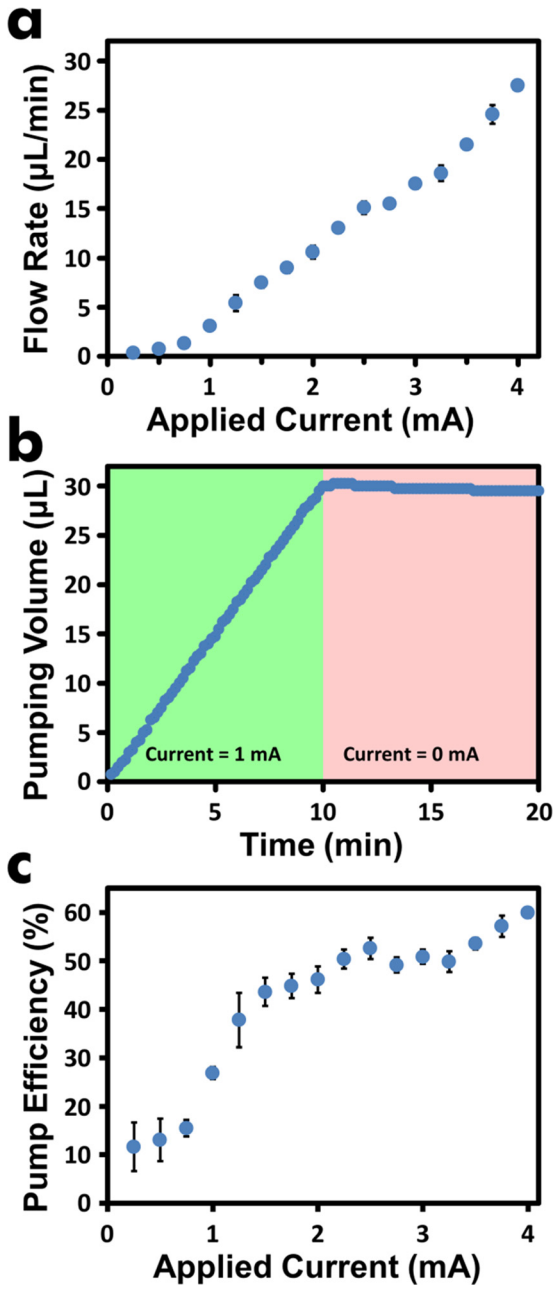

FIG. 3. (a) Characterization of the electrolytic micropump flow rate with the amount of current applied. (b) Electrolytic micropump is operated at 1 mA for 10 min with a steady increase in measured pumped volume. Current is off between 10 and 20 min time point. (c) Micropump efficiency is determined at applied current up to 4 mA.

(t) in seconds. In the case of the applied electrolyte current of 1 mA, it would lead to 0.19 μl of gas generation in 1 s.[42] To obtain $V_{experimental}$, the electrolytic micropump is fabricated to pump fluid into a channel that opens to the room environment. Current is applied for 60 s and the distance of fluid front is measured and converted to the volume displaced. Combining Eqs. (1) and (2), the electrolytic efficiency can be determined and has been plotted in Fig. 3(c) as a function of the applied current. As can be seen, the pumping efficiency rapidly increases from 10% to 43% with the electric current strength at a lower current level of 0 to 1.5 mA. From 1.5 mA and above, pumping efficiency rises slowly until reaching the maximal efficiency value of 60% at 4.0 mA. The electrolytic micropump can be further optimized by smaller electrode configuration that provides larger current density and faster bubble nucleation.[54]

D. Mobile-interfaced immunoassay operation

We have demonstrated the working principle of an on-chip automated immunoassay operation on our microfluidic device integrated with C-PDMS electrolytic micropump. In this microfluidic assay, we intend to detect BDE-47 (2,2′,4,4′-tetrabromodiphenyl ether) and calibrate the signal readout using known concentration of samples in an aqueous buffer. As a wide spread type of flame retardant PBDEs, BDE-47 has been contained in many manufactured products such as plastics, electronics, and textiles that may have a significant health impact on humans and the environment.[55] The negative effects of PBDEs have forced the ban of this type of substances, which have already been prominently found in many human blood samples.[56] Therefore, point-of-care detection of the presence of PBDEs in a potentially contaminated area is a critical demand.

As previously described in Sec. II, prior to running ELISA detection of BDE-47, the electrolytic micropumps are primed with 0.5 M KNO_3 via needle injection. Once ready, sample solutions containing known concentrations of BDE-47 analytes (10^{-3}–10^{4} μg/l) are mixed with VHH, referred to as αBDE-47 (4 μg/l). One advantage of using VHH over conventional antibodies is because of their single domain nature allowing them to be highly amenable to genetic manipulation and expression in various systems.[57,58] Heat stability is another feature of VHH especially applicable in mobile POC diagnostics as temperature may fluctuate during travel and geographic locations.[45] Additionally, the storage condition of ELISA devices is less of a constraint. Here, HRP is directly conjugated to our VHH, eliminating the downstream step of using secondary antibodies for visualization. The VHH/analyte mixture (2 μl) is loaded into the red circular chamber/channel as indicated in Fig. 4(a). Once the mixture is loaded, the ELISA process becomes completely automated driven by the Arduino microprocessor. The first pump (red) transport the VHH/analyte mixture to the detection chamber (green), where an incubation of 10 min takes place. A second pump (blue) containing buffer washes the detection chamber to remove all unbound VHHs. Lastly, the third pump (yellow) delivers enzymatic substrate to the detection chamber for colorimetric reaction to occur with bound HRP-conjugated VHHs. Aside from transmitting the data to a computer for processing, the internal computing capability of the smartphone can be used instead if a proper application (app) is specifically developed. Fig. 4(b) shows a photograph of the microfluidic ELISA device. The channels are colored red for visualization purposes and the inset shows a close-up view of a single electrolytic micropump with interdigitated C-PDMS electrodes. The ELISA device fits onto an encased copper PCB with Arduino Nano (supplementary material).[61]

The performances of competitive ELISA in LOC and conventional laboratory formats are compared in Fig. 4(c). Colorimetric signals from sample analyte have signals from BSA control subtracted and then normalized to scales the two curves for comparison. See the supplementary material for images of ELISA colorimetric signal in the microfluidic detection chamber.[61] Performance results show comparable matching signal strength in 10^{1}–10^{3} μg/l concentration range. The calibration curve for the on-chip procedure shows a shift to the left (in 10^{-3}–10^{1} μg/l concentration range) when compared to the conventional assay resulting in a more sensitive assay due to the combination of smaller volume and faster reaction time, given the principle of competitive ELISA specifically beneficial at the lower concentration spectrum. In the on-chip microfluidic ELISA format, the micro/nano dimensions of channels and chambers enhance binding of antibodies to the antigens on the surface of device as the distance antibodies need to travel is shortened. As comparison, at the same concentration, antibodies in the bulk may never reach the surface antigens to be detected in the conventional format. Thus, we have observed a more sensitive system using the on-chip microfluidic ELISA. The shift in the curve is more drastic in 10^{-3}–10^{1} μg/l range than that of 10^{1}–10^{4} μg/l, because competitive ELISA is conceptually designed to be more distinguishable at lower concentrations ($<10^{1}$ μg/l).[59,60] Briefly, at a low concentration of sample antigen, antibody concentration in solution is high and the molecules are readily to bind to surface antigens within a short diffusion length. In addition, the LOC assay has a significant faster readout time of 15 min compared to conventional ELISAs which typically take at least 2 h. The plate preparation includes 1 h coating and 1 h blocking.

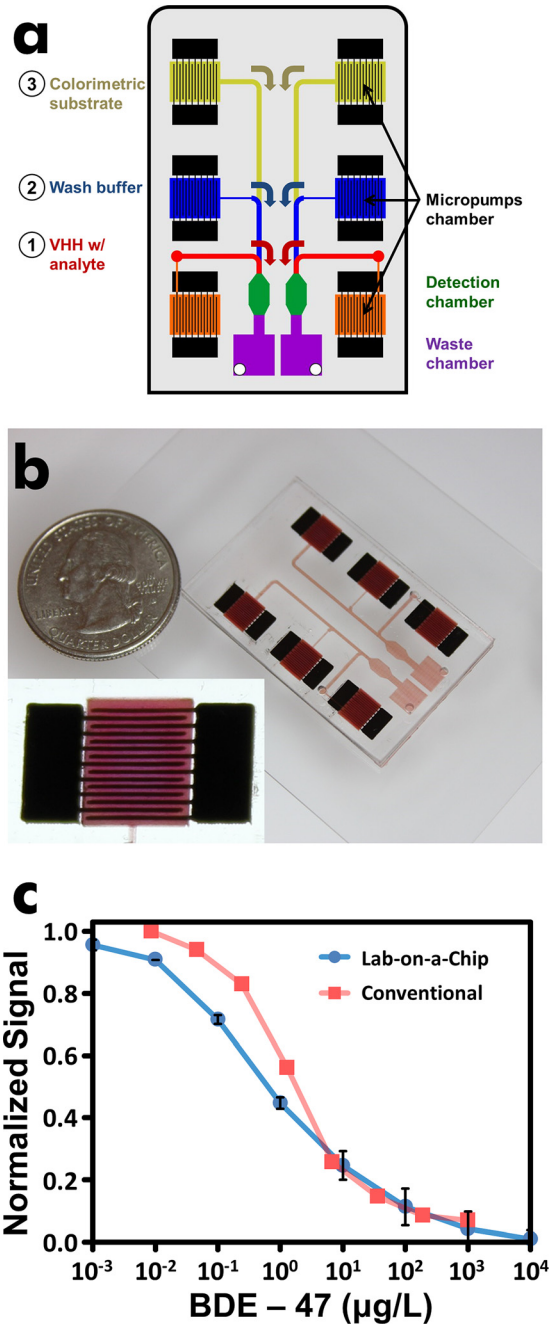

FIG. 4. (a) An illustration of the microfluidic ELISA device with flow operations from three micropumps. (b) A photograph of the microfluidic ELISA device filled with colored solution for visualization. (Inset) A close-up of the interdigitated carbon-PDMS electrodes under the micropump chamber. (c) Characterization of the BDE-47 detection profile in the microfluidic ELISA device and the conventional ELISA assay process. Signals are normalized and standard deviation bars are shown (with n = 3).

After preparation, the ELISA process includes 1 h for antibody-antigen binding, 1 h for secondary antibody binding, 5 min wash steps, and 15 min for colorimetric development. Using HRP directly conjugated to the primary antibody, VHH, time required for binding secondary antibodies is eliminated. In addition, at low volume scale ($<\mu$l) within microfluidic reaction chambers, kinetics of enzymatic reactions reaches completion faster due to close vicinity of molecules. In comparison, standard ELISA cannot be achieved within a 15-min time window, as the required

antibody-antigen binding may not be completed. In addition, evaporation of liquid can become a problem when using a small volume in a standard ELISA procedure, where all the chemicals are exposed to the environment. The input sample volume is considerably reduced to 2 μl in the LOC device from a 50 μl requirement in the laboratory ELISA. This allows the LOC assay device to be field-deployable in a point-of-care fashion to analyze less-than-ideal samples that the conventional method is insensitive and incapable to detect. The overall detection assay enables an immediate readout through VHH implementation and a minimal sample volume for the monitoring of BDE-47 environment contaminant.

IV. CONCLUSIONS

In this paper, we present a low-cost, portable microfluidic competitive ELISA system for the mobile detection of a common environmental contaminant, BDE-47 (2,2′,4,4′-tetrabromodiphenyl ether), as an example. Our generic lab-on-a-chip system consists of an Arduino-compatible microcontroller integrated with a PCB, a microfluidic ELISA chip, and a smartphone interface. The microfluidic ELISA device converts electronic current input into a fluid flow for pumping fluidics in a biochemical system through the use of carbon black/PDMS (C-PDMS) composite electrodes. The conductivity of the C-PDMS material has been characterized for composite containing 5%–25% carbon. Furthermore, flow characteristics of C-PDMS micropump have been investigated and integrated into an on-chip immunoassay device for the detection of environmental contaminant BDE-47. The microfluidic ELISA device is described and its detection responses for BDE-47 have been measured to have a detection range of 10^{-3}–10^{4} μg/l using VHH (single domain antibodies or Nanobodies), with a comparable performance to that uses a standard ELISA protocol. Importantly, the platform is not limited only to BDE-47 detection as the immunoassay antigen proteins can be substituted for another target to permit other applications. The low-cost and health benefit aspect of our system are suitable for rural or less developed regions, and the mobile aspect allows the point-of-care health diagnosis and environmental safety monitoring to be readily deployed for a wide user basis in the near future.

ACKNOWLEDGMENTS

This work was in part supported by the NSF CAREER Award No. (ECCS-0846502) and National Institutes of Environmental Health Sciences of NIH Superfund Research Program (No. P42ES004699). We thank Philip Digiglio for his assistance on programming the Arduino microcontroller and Shirley Gee for reviewing the manuscript.

[1]A. Ozcan, Lab Chip **14**(17), 3187–3194 (2014).
[2]See http://www.itu.int/en/ITU-D/Statistics/Documents/facts/ICTFactsFigures2014-e.pdf for International Telecommunication Union, ICT Facts and Figures, 2014 (accessed 28 August 2014).
[3]A. Kailas, C. C. Chong, and F. Watanabe, IEEE Pulse **1**(1), 57–63 (2010).
[4]J. M. Kelly, R. E. Strecker, and M. T. Bianchi, ISRN Neurol. **2012**, 768794.
[5]M. J. Gregoski, M. Mueller, A. Vertegel, A. Shaporev, B. B. Jackson, R. M. Frenzel, S. M. Sprehn, and F. A. Treiber, Int. J. Telemed. Appl. **2012**, 696324.
[6]A. W. Martinez, S. T. Phillips, E. Carrilho, S. W. Thomas III, H. Sindi, and G. M. Whitesides, Anal. Chem. **80**(10), 3699–3707 (2008).
[7]Y. Lu, W. Shi, J. Qin, and B. Lin, Electrophoresis **30**(4), 579–582 (2009).
[8]H. Zhu, O. Yaglidere, T. W. Su, D. Tseng, and A. Ozcan, Lab Chip **11**(2), 315–322 (2011).
[9]H. Zhu, S. Mavandadi, A. F. Coskun, O. Yaglidere, and A. Ozcan, Anal. Chem. **83**(17), 6641–6647 (2011).
[10]H. Zhu, I. Sencan, J. Wong, S. Dimitrov, D. Tseng, K. Nagashima, and A. Ozcan, Lab Chip **13**(7), 1282–1288 (2013).
[11]P. B. Lillehoj, M. C. Huang, N. Truong, and C. M. Ho, Lab Chip **13**(15), 2950–2955 (2013).
[12]Q. Wei, R. Nagi, K. Sadeghi, S. Feng, E. Yan, S. J. Ki, R. Caire, D. Tseng, and A. Ozcan, ACS Nano **8**(2), 1121–1129 (2014).
[13]C. D. Chin, T. Laksanasopin, Y. K. Cheung, D. Steinmiller, V. Linder, H. Parsa, J. Wang, H. Moore, R. Rouse, G. Umviligihozo, E. Karita, L. Mwambarangwe, S. L. Braunstein, J. van de Wijgert, R. Sahabo, J. E. Justman, W. El-Sadr, and S. K. Sia, Nat. Med. **17**(8), 1015–1019 (2011).
[14]Y. H. Lin, Y. J. Chen, C. S. Lai, Y. T. Chen, C. L. Chen, J. S. Yu, and Y. S. Chang, Biomicrofluidics **7**(2), 024103 (2013).
[15]J. Kai, A. Puntambekar, N. Santiago, S. H. Lee, D. W. Sehy, V. Moore, J. Han, and C. H. Ahn, Lab Chip **12**(21), 4257–4262 (2012).
[16]S. Sun, M. Yang, Y. Kostov, and A. Rasooly, Lab Chip **10**(16), 2093–2100 (2010).
[17]T. Ohashi, K. Mawatari, K. Sato, M. Tokeshi, and T. Kitamori, Lab Chip **9**(7), 991–995 (2009).

[18]P. Novo, D. M. Prazeres, V. Chu, and J. P. Conde, Lab Chip **11**(23), 4063–4071 (2011).
[19]S. Senapati, A. R. Mahon, J. Gordon, C. Nowak, S. Sengupta, T. H. Q. Powell, J. Feder, D. M. Lodge, and H. C. Chang, Biomicrofluidics **3**(2), 022407 (2009).
[20]Y. S. Wang, T. C. Chang, P. R. Stoddart, and H. C. Chang, Biomicrofluidics **8**(2), 021101 (2014).
[21]B. D. Iverson and S. V. Garimella, Microfluid. Nanofluid. **5**(2), 145–174 (2008).
[22]F. Amirouche, Y. Zhou, and T. Johnson, Microsyst. Technol. **15**(5), 647–666 (2009).
[23]A. Volanschi, W. Olthuis, and P. Bergveld, Sens. Actuators, A **52**(1–3), 18–22 (1996).
[24]D. Okeefe, C. Oherlihy, Y. Gross, and J. G. Kelly, Br. J. Anaesth. **73**(6), 843–846 (1994).
[25]C. R. Neagu, J. G. E. Gardeniers, M. Elwenspoek, and J. J. Kelly, J. Microelectromech. Syst. **5**(1), 2–9 (1996).
[26]C. Belmont and H. H. Girault, J. Appl. Electrochem. **24**(6), 475–480 (1994).
[27]S. Bohm, W. Olthuis, and P. Bergveld, Biomed. Microdevices **1**(2), 121–130 (1999).
[28]S. Bohm, B. Timmer, W. Olthuis, and P. Bergveld, J. Micromech. Microeng. **10**(4), 498–504 (2000).
[29]V. I. Furdui, J. K. Kariuki, and D. J. Harrison, J. Micromech. Microeng. **13**(4), S164–S170 (2003).
[30]C. G. Cameron and M. S. Freund, Proc. Natl. Acad. Sci. U.S.A. **99**(12), 7827–7831 (2002).
[31]S. Z. Hua, F. Sachs, D. X. Yang, and H. D. Chopra, Anal. Chem. **74**(24), 6392–6396 (2002).
[32]J. Xie, Y. N. Miao, J. Shih, Q. He, J. Liu, Y. C. Tai, and T. D. Lee, Anal. Chem. **76**(13), 3756–3763 (2004).
[33]H. V. Fuentes and A. T. Woolley, Lab Chip **7**(11), 1524–1531 (2007).
[34]S. H. Chiu and C. H. Liu, Lab Chip **9**(11), 1524–1533 (2009).
[35]G. Blanco-Gomez, A. Glidle, L. M. Flendrig, and J. M. Cooper, Anal. Chem. **81**(4), 1365–1370 (2009).
[36]P. Y. Li, J. Shih, R. Lo, S. Saati, R. Agrawal, M. S. Humayun, Y. C. Tai, and E. Meng, Sens. Actuators, A **143**(1), 41–48 (2008).
[37]W. Li, D. C. Rodger, E. Meng, J. D. Weiland, M. S. Humayun, and Y. C. Tai, J. Microelectromech. Syst. **19**(4), 735–742 (2010).
[38]H. Gensler, R. Sheybani, P. Y. Li, R. Lo Mann, and E. Meng, Biomed. Microdevices **14**(3), 483–496 (2012).
[39]A. Takashima, K. Kojima, and H. Suzuki, Anal. Chem. **82**(16), 6870–6876 (2010).
[40]W. Satoh, Y. Shimizu, T. Kaneto, and H. Suzuki, Sens. Actuators, B **123**(2), 1153–1160 (2007).
[41]Y. Shimizu, A. Takashima, W. Satoh, F. Sassa, J. Fukuda, and H. Suzuki, Sens. Actuators, B **140**(2), 649–655 (2009).
[42]J. Nestler, A. Morschhauser, K. Hiller, T. Otto, S. Bigot, J. Auerswald, H. F. Knapp, J. Gavillet, and T. Gessner, Int. J. Adv. Manuf. Technol. **47**(1–4), 137–145 (2010).
[43]A. L. Deman, M. Brun, M. Quatresous, J. F. Chateaux, M. Frenea-Robin, N. Haddour, V. Semet, and R. Ferrigno, J. Micromech. Microeng. **21**(9), 095013 (2011).
[44]B. Mustin and B. Stoeber, Lab Chip **12**(22), 4702–4708 (2012).
[45]C. R. Bever, Z. Majkova, R. Radhakrishnan, I. Suni, M. McCoy, Y. Wang, J. Dechant, S. Gee, and B. D. Hammock, Anal. Chem. **86**(15), 7875–7882 (2014).
[46]K. C. Ahn, S. J. Gee, H. J. Tsai, D. Bennett, M. G. Nishioka, A. Blum, E. Fishman, and B. D. Hammock, Environ. Sci. Technol. **43**(20), 7784–7790 (2009).
[47]H. J. Kim, M. R. McCoy, Z. Majkova, J. E. Dechant, S. J. Gee, S. Tabares-da Rosa, G. G. Gonzalez-Sapienza, and B. D. Hammock, Anal. Chem. **84**(2), 1165–1171 (2012).
[48]B. Samel, M. K. Chowdhury, and G. Stemme, J. Micromech. Microeng. **17**(8), 1710–1714 (2007).
[49]M. A. Eddings, M. A. Johnson, and B. K. Gale, J. Micromech. Microeng. **18**(6), 067001 (2008).
[50]B. M. A. Henriques, R. J. Mistri, and M. M. Johri, J. Biosci. **23**(2), 111–118 (1998).
[51]X. Z. Niu, S. L. Peng, L. Y. Liu, W. J. Wen, and P. Sheng, Adv. Mater. **19**(18), 2682 (2007).
[52]I. Balberg, Carbon **40**(2), 139–143 (2002).
[53]H. L. Cong, L. F. Hong, R. S. Harake, and T. R. Pan, J. Micromech. Microeng. **20**(2), 025002 (2010).
[54]D. A. Ateya, A. A. Shah, and S. Z. Hua, Rev. Sci. Instrum. **75**(4), 915–920 (2004).
[55]B. C. Kelly, M. G. Ikonomou, J. D. Blair, A. E. Morin, and F. A. Gobas, Science **317**(5835), 236–239 (2007).
[56]D. B. Barr, A. O. Olsson, L. Y. Wong, S. Udunka, S. E. Baker, R. D. Whitehead, M. S. Magsumbol, B. L. Williams, and L. L. Needham, Environ. Health Perspect. **118**(6), 742–748 (2010).
[57]M. A. Ghahroudi, A. Desmyter, L. Wyns, R. Hamers, and S. Muyldermans, FEBS Lett. **414**(3), 521–526 (1997).
[58]M. M. Harmsen and H. J. De Haard, Appl. Microbiol. Biotechnol. **77**(1), 13–22 (2007).
[59]S. D. Gan and K. R. Patel, J. Invest. Dermatol. **133**(9), E10–E12 (2013).
[60]E. Dobrovolskaia, A. Gam, and J. E. Slater, Clin. Exp. Allergy **36**(4), 525–530 (2006).
[61]See supplementary material at http://dx.doi.org/10.1063/1.4901348 for the encased Arduino microcontroller with a microfluidic chip slot and colorimetric images of the ELISA reaction in the microfluidic detection chamber.